Vaccine 37 (2019) 7070–7080

Contents lists available at ScienceDirect

Vaccine

journal homepage: www.elsevier.com/locate/vaccine

Polymer-grafted chromatography media for the purification of enveloped virus-like particles, exemplified with HIV-1 gag VLP

Patricia Pereira Aguilar [a], Tobias Amadeus Schneider [b], Viktoria Wetter [b], Daniel Maresch [a], Wai Li Ling [c], Andres Tover [d], Petra Steppert [a], Alois Jungbauer [a,b,*]

[a] Department of Biotechnology, University of Natural Resources and Life Sciences Vienna, Austria
[b] Austrian Centre of Industrial Biotechnology, Vienna, Austria
[c] Univ. Grenoble Alpes, CEA, CNRS, IBS, F-38000 Grenoble, France
[d] Icosagen AS, Tartumaa, Estonia

ARTICLE INFO

Article history:
Available online 9 July 2019

Keywords:
Fractogel®
Dynamic binding capacity
HIV-1 gag variants
Nanoparticle tracking analysis
Multi-angle light scattering

ABSTRACT

Polymer-grafted chromatography media, especially ion exchangers, are high performance materials for protein purification. However, due to the pore size limitation, conventional chromatography beads are usually not considered for the downstream processing of large biomolecules such as virus-like particles (VLPs). Contrariwise, since the outer surface of the chromatography beads provides satisfactory binding capacity for VLPs and impurities of smaller size can bind inside of the beads, conventional porous beads should be considered for VLP capture and purification. We used HIV-1 gag VLPs with a diameter of 100–200 nm as a model to demonstrate that polymer-grafted anion exchangers are suitable for the purification of bionanoparticles. The equilibrium binding capacity was 1×10^{13} part/mL resin. Moderate salt concentration up to 100 mM NaCl did not affect binding, allowing direct loading of cell culture supernatant onto the column for purification. Dynamic binding capacity at 10% breakthrough, when loading cell culture supernatant, was approximately 6×10^{11} part/mL column; only 1-log lower than for monoliths. Endonuclease treatment of the cell culture supernatant did not increase the dynamic binding capacity, suggesting that dsDNA does not compete for the binding sites of VLPs. Nevertheless, due to simultaneous elution of particles and dsDNA, endonuclease treatment is required to reduce dsDNA contamination in the product. Proteomic analysis revealed that HIV-1 gag VLPs contain different host cell proteins in their cargo. This cargo is composed of conserved proteins and other proteins that vary from one particle population to another, as well as from batch to batch. This process allowed the separation of different particle populations. HIV-1 gag VLPs were directly captured and purified from cell culture supernatant with a total particle recovery in the elution of about 35%. Columns packed with beads can be scaled to practically any dimension and therefore a tailored design of the process is possible.
© 2019 The Authors. Published by Elsevier Ltd. This is an open access article under the CC BY license (http://creativecommons.org/licenses/by/4.0/).

1. Introduction

Polymer-grafted chromatography media are rigid porous backbone supports containing polymer chains grafted on their surface. In ion exchange chromatography, these polymer chains are functionalized with charged ligands, which are responsible for interacting with biomolecules [1]. Ion-exchange chromatography is a highly efficient unit operation for the purification of biopharmaceuticals such as proteins, DNA and bionanoparticles [2–4]. Currently emerging biopharmaceuticals include very large and complex molecules, with hydrodynamic radius ranging from tens to hundreds of nanometers, such as virus-like particles (VLPs), viral vectors, extracellular vesicles (EVs) and liposomes [5–11]. New generation matrices have been developed for the capture and purification of such large bionanoparticles including monoliths, membrane adsorbers, fibers and gigaporous resins [8,12,13]. Monoliths', membrane adsorbers' and fibers' open pore structure results in higher surface area available for the binding of large biomolecules and the predominant convective mass transfer allows the use of high flow rates [14–16]. However, monoliths are prone to fouling and clogging and membrane adsorbers tend to have poor resolution [12,17]. Additionally, although these type of matrices can be scaled-up, they are produced in a limited number of sizes reducing the flexibility of the scale-up. Conversely, conventional

* Corresponding author at: Department of Biotechnology, University of Natural Resources and Life Sciences Vienna, Muthgasse 18, 1190 Vienna, Austria.
E-mail address: alois.jungbauer@boku.ac.at (A. Jungbauer).

https://doi.org/10.1016/j.vaccine.2019.07.001
0264-410X/© 2019 The Authors. Published by Elsevier Ltd.
This is an open access article under the CC BY license (http://creativecommons.org/licenses/by/4.0/).

chromatography media (beads) have the advantage of easy and flexible scalability to industrial scale [18]. Porous beads are usually not considered for the purification of large biomolecules in bind-elute mode due to pore size limitations. As a rule of thumb, it is assumed that to guarantee fast mass transfer, a pore size 10 times larger than the molecule size is required [19,20]. Macro- and giga-porous chromatography beads were developed to overcome the mass transfer limitation of conventional porous beads. Yu et al. showed that increasing the resin's pore diameter (up to 280 nm) increases both, binding capacity and mass transfer rate of HB-VLPs (50 nm diameter) [21]. Still, the estimated effective pore diffusivity (D_e) was one or two orders of magnitude lower than the D_e of most proteins in similar conditions [22]. Moreover, larger biomolecules (diameter >50 nm) are usually excluded from the resin pores, binding as thin layers on the surface of the beads and consequently resulting in lower binding capacities [23,24]. Nevertheless, the expected reduced binding capacity of large biomolecules onto porous chromatography beads can be balanced by the easy scalability of this type of chromatography. In addition, binding sites in the interior of the beads are available for binding of impurities such as host cell proteins, DNA and RNA, reducing the probability of binding site competition and displacement effects.

Polymer-grafted ion exchangers are widely used for protein purification and have higher binding capacity when compared to non-grafted resins [25,26]. This is explained by the increase in surface area and ligand density upon grafting (up to a certain limit), as well as by the 3D structure of the ligands which allows multilayer adsorption [26–28]. To investigate the applicability of ion exchange chromatography beads for the purification of large and complex biomolecules we used Fractogel® EMD TMAE Hicap (M) resin from Merck (Darmstadt, Germany), hereinafter referred as Fractogel®-TMAE. Fractogel®-TMAE beads have a crosslinked polymethacrylate backbone grafted with long linear polymer chains ("tentacles") which are functionalized with trimethylaminoethyl groups (strong anion exchanger). Ligands in tentacle-type ion exchangers have high flexibility allowing multipoint ligand-biomolecule interactions. This increases selectivity as the interaction involves the overall steric charge distribution of the biomolecules [29,30]. According to the manufacturer, Fractogel®-TMAE beads have a particle size distribution of 40–90 μm and a pore size of 80 nm.

Within the new emerging biopharmaceuticals, we selected enveloped virus-like particles (eVLPs) as model for large and complex biomolecules. VLPs have proven their value in several applications such as vaccines, drug delivery and medical diagnostics [5,6,9,31]. VLPs have the advantageous safety profile of subunit vaccines (lack of viral genetic material) while keeping the same efficacy of the conventional ones, such as killed or live attenuated vaccines [7,31]. Enveloped virus-like particles are formed in a complex process which includes the self-assembly of recombinant viral proteins while budding at a host cell membrane. It has been shown that, besides the plasma membrane, several intracellular membranes, such as endosomes, nuclear envelope, endoplasmic reticulum and Golgi, serve as viral budding platforms [32]. Due to the complexity of the assembly and budding processes, the recombinant production of eVLPs often results in heterogeneous particle population's, which may include in their cargo (incorporated molecular components) different host cell proteins, DNA and/or RNA fragments [33–35]. Additionally, cells naturally release extracellular vesicles (EVs) with similar surface properties, size, structure and cargo to eVLPs because both, eVLPs and EVs, share some biogenesis pathways [36]. The result is a very complex mixture containing different bionanoparticle populations that need to be separated in order to allow their characterization and understanding of their biologic activity. Since eVLPs are surrounded by the host cell lipid-bilayer it is assumed that they have multiple positive and negative charges on their surface [37]. We used HIV-1 gag VLPs, produced in CHO cells, which have a diameter of about 100–200 nm. Steppert et al. showed that HIV-1 gag VLPs bind to anion exchange monoliths but do not bind to cation exchange monoliths, revealing that these VLPs have an overall negative net charge (in a pH range from 6.5 to 8.5) [38]. Therefore, HIV-1 gag VLPs are suitable for investigating the capability of polymer-grafted anion exchangers, such as Fractogel®-TMAE, to capture and purify eVLPs.

A remaining challenge in the development and optimization of downstream processes is the lack of high throughput methodologies for specific detection and quantification of eVLPs in complex mixtures, as well as for the in-process control of product quality and quantity [6,39]. Additionally, there are no simple and accurate bioassay for differentiating between different particle populations [40,41]. So far the available methods for EV and VLP discrimination depend on modifications at the cellular level, for example by incorporating fluorescent tags in VLPs [42,43]. Thus, we used a combination of methods for particle detection, quantification and visualization (multi-angle light scattering, MALS; nanoparticle tracking analysis, NTA; TEM and cryo-TEM), total and specific protein detection and quantification (SDS-PAGE, Bradford assay, Western blot analysis and ELISA) and dsDNA quantification (Picogreen assay). Proteomic analysis (mass spectrometry) was performed to characterize the cargo of the particles and differentiate different particle populations.

We developed a downstream processing strategy based on polymer-grafted chromatography media (Fractogel®-TMAE) for the direct capture and purification of HIV-1 gag VLPs and separation of different particle populations.

2. Materials and methods

2.1. Chemicals and reagents

Chemicals and reagents used in the experiments were purchased from Merck KGaA (Darmstadt, Germany) or Sigma Aldrich (St. Louis, MO, USA).

2.2. HIV-1 gag VLPs

Cell culture supernatant containing HIV-1 gag VLPs was kindly provided by Icosagen (Tartumaa, Estonia). The VLPs were produced in a CHOEBNALT85 cell line using a stable episomal expression system, as previously described by Steppert et al. [1].

2.3. Endonuclease treatment

The digestion of double stranded DNA (dsDNA) was performed using Benzonase® purity grade II (Merck KGaA, Darmstadt Germany) according to the manufacturer's instructions. Briefly, the clarified cell culture supernatant was treated with 150 U/mL Benzonase® and 2 mM $MgCl_2$ for 2 h at 37 °C.

2.4. Adsorption isotherms

Adsorption isotherms were determined by equilibrating 10 μL of Fractogel®-TMAE (Fractogel® EMD TMAE Hicap (M) resin, Merck, Darmstadt, Germany) with 250 μL HIV-1 gag VLP solutions, at different initial concentrations, in 96 well filter plates (AcroPrep™ Advance, 350 μL, 1.2 μm Supor® membrane, Pall Corporation, New York, USA). For this purpose, HIV-1 gag VLPs were purified by preparative anion exchange chromatography using an 8 mL CIMmultus QA monolith (BIA Separations, Ajdovščina, Slovenia) as previously described by Steppert et al. [38]. Purified VLPs were

buffer exchanged to 50 mM HEPES, pH 7.2 buffer containing 0 or 100 mM NaCl using Slide-A-Lyzer™ Dialysis Cassettes (Thermo Fisher Scientific, Waltham, MA, USA) with a 10 K molecular weight cut off. Fractogel®-TMAE was equilibrated with the same buffer conditions as the VLPs. All isotherms were conducted at 22 °C and 350 rpm during 24 h. After equilibration, a filtration step was used to separate the resin from the equilibrium VLP solution (containing the unbound VLPs). VLP quantification before and after equilibration with the resin was performed by measuring the UV absorbance at 280 nm. A calibration curve relating the particle concentration measured by Nanoparticle Tracking Analysis (NTA) and the UV absorbance at 280 nm was used to access the VLP concentration in particles/mL.

2.5. Chromatographic experiments

2.5.1. Equipment

Chromatographic experiments were performed on an Äkta pure 25 M2 equipped with a 1.4 mL mixer chamber, a S9 sample pump and a F9-C fraction collector (GE Healthcare, Uppsala, Sweden). System control and data acquisition were performed using the Unicorn 6.4.1 software. UV absorbance (280, 260 and 214 nm), conductivity and pH were continuously monitored during the chromatographic runs.

2.5.2. Chromatographic stationary and mobile phases

Fractogel®-TMAE (Fractogel® EMD TMAE Hicap (M) resin) was used as stationary phase (Merck KGaA, Darmstadt, Germany). Buffer A, containing 50 mM HEPES, pH 7.2 and buffer B, containing 50 mM HEPES, 2 M NaCl, pH 7.2 were used as mobile phases. To obtain different concentration of the modifier (NaCl), buffer A and B were mixed. During cleaning-in-place procedures, 0.5 M NaOH was used. All buffers were prepared with ultra-pure water and filtered using MF-Millipore™ 0.22 μm MCE Membranes (Sigma Aldrich, St. Louis, MO, USA).

2.5.3. Breakthrough curves and dynamic binding capacity

Breakthrough experiments were performed in prepacked Mini-Chrom columns 8 × 20 mm (Merck KGaA, Darmstadt, Germany) containing 1 mL of Fractogel®-TMAE. Clarified cell culture supernatant was 0.8 μm filtered (Millex AA filter, Millipore Bedford, USA) and, without further preconditioning, loaded into the column. The used method consisted of a 10 CV equilibration step at 5% B, followed by the injection of 50 mL loading material via sample pump. The flow rate was 0.2 mL/min (24 cm/h, 5 min residence time). Flow-through fractions were collected and pooled according to the chromatogram. The same method was used for the breakthrough curve of endonuclease treated cell culture supernatant. The dynamic binding capacity ($DBC_{10\%}$) was calculated at 10% breakthrough of particles in the range of 100–200 nm (measured with NTA). $DBC_{10\%}$ was calculated using the following equation $DBC_{10\%} = (C_F \cdot V_{b,10\%})/CV$, where C_F is the feed concentration, $V_{b,10\%}$ is the load volume at 10% breakthrough and CV is the column volume [18].

2.5.4. Purification of HIV-1 gag VLPs

For preparative purification of HIV-1 gag VLPs form CHO cell culture supernatant, a XK 16/20 column (GE Healthcare, Uppsala, Sweden) packed with 5.43 mL of Fractogel®-TMAE was used. Clarified cell culture supernatant (or clarified and Benzonase® treated cell culture supernatant) was 0.8 μm filtered (Millex AA filter, Millipore Bedford, USA) and, without further preconditioning, loaded into the column. The used method consisted of a 2 CV equilibration step at 5% B, followed by the injection of 50 mL loading material via sample pump. After loading, the column was washed with 5% B buffer for 6 CV. Elution was achieved by a salt linear gradient from 5 to 50% B in 20 CV, including a 10 mL hold step at 50% B at the end of the gradient. The column was regenerated with 100% B in a 3 CV step. Cleaning-in-place (CIP) was performed with 0.5 M NaOH in a 5 CV step. The flow rate was 1.0 mL/min (29.8 cm/h, 5.4 min residence time). Small fractions were collected in 96-well plates during the whole run and pooled according to the chromatogram.

2.6. Multi-angle light scattering (MALS)

Light scattering intensity (LS) measurements were performed using a MALS detector (DAWN HELEOS, 18-angle, Wyatt, Santa Barbara, CA, USA) connected to an Ultimate 3000 HPLC system equipped with a 3000TSL autosampler (Thermo Fisher, Waltham, MA, USA). Chromeleon® 7 software (Thermo Fisher, Waltham, MA, USA) was used to control the HPLC system. LS data was acquired and processed using the ASTRA software, version 6.1.2 (Wyatt, Santa Barbara, CA, USA). A sample volume of 20 μL was directly injected into the MALS detector using the HPLC in bypass mode. All samples were measured in duplicates. A flow rate of 0.3 mL/min was used.

2.7. Nanoparticle tracking analysis (NTA)

Particle concentration and particle size distribution were determined by NTA using a NanoSight NS300 instrument (Malvern Instruments Ltd., Worcestershire, UK), equipped with a blue laser module (488 nm) and a neutral density filter. The NanoSight NTA software version 3.2 (Malvern Instruments Ltd., Worcestershire, UK) was used for instrument control, data acquisition and data processing. Each sample was serially diluted in particle-free water in order to obtain a particle concentration in the range of 20–100 particles/frame. For each sample, three dilutions were measured. Per dilution, five videos of 30 s were recorded and analysed. All measurements were performed at 25 °C. The camera level was manually adjusted to values between 12 and 16. For the data processing, detection thresholds between 3 and 5 were used. Remaining analysis parameters were automatically selected by the software and kept constant for all samples.

2.8. Total protein and double stranded DNA (dsDNA) quantification

Total protein was quantified by Bradford assay using Coomassie blue G-250-based protein dye reagent (Bio-Rad Laboratories, Hercules, CA, USA). Bovine serum albumin (BSA) standards (Thermo Fisher Scientific, Waltham, MA, USA) diluted in 1x PBS buffer were used to obtain a calibration curve in the range of 25–200 μg/mL. Total dsDNA was quantified using Quant-iT™ PicoGreen® dsDNA kit (Life Technologies, Waltham, MA, USA). Both quantifications were performed in a microtiter plate format according to the manufacturer's instructions. A Genius Pro plate reader (Tecan, Männedorf, Switzerland) was used to measure the signals in both assays.

2.9. Protein identification and peptide analysis using LC-ESI-MS

Relevant samples were digested with sequencing grade modified trypsin (Promega, Madison, Wisconsin, EUA). The samples were analysed using a Dionex Ultimate 3000 system (Thermo Fischer Scientific, Waltham, MA, USA) directly linked to a QTOF instrument (maXis 4G ETD, Bruker, Billerica, Massachusetts, USA) equipped with the standard ESI source (CaptiveSpray nanoBooster, respectively) in the positive ion, DDA mode (=switching to MSMS mode for eluting peaks). MS-scans were recorded (range: 150–2200 m/z) and the 6 highest peaks were selected for fragmentation. Instrument calibration was performed using ESI calibration mixture (Agilent Technologies, Santa Clara, California, EUA). For separation of the peptides a Thermo BioBasic C18 separation

column (5 μm particle size, 150 × 0.320 mm) was used. A gradient from 95% solvent A and 5% solvent B (Solvent A: 65 mM ammonium formiate buffer, B: 100% ACN) to 32% B in 45 min was applied, followed by a 15 min gradient from 32% B to 75% B, at a flow rate of 6 μL/min. For the measurements in nano-mode a Thermo Acclaim PepMap300 RSLC C18 separation column (2 μm particle size, 150 × 0.075 mm) was used with a Thermo Acclaim PepMap μ-precolumn. A gradient from 5% solvent B (solvent A: 0.1% formic acid in HQ-water, solvent B: 0.1% formic acid in ACN) to 32% B in 60 min was applied, followed by a 10 min gradient from 32% B to 70% B that facilitates elution of large peptides, at a flow rate of 0.3 μL/min. The analysis files were converted using Data Analysis 4.0 (Bruker, Billerica) to XML files, which are suitable to perform MS/MS ion searches with MASCOT (embedded in ProteinScape 3.0, Bruker) for protein identification. Only proteins identified with at least 2 peptides with a protein score higher than 80 were accepted. For the searches, the reviewed UniProt database and the Reference proteome of Cricetulus griseus (UP000001075) were used.

2.10. Enzyme-linked immunosorbent assay (ELISA)

The HIV-1 p24 Capsid Protein p24 ELISA Kit (Sino Biological, Wayne, USA) was used for the quantification of HIV-1 p24, which is part of the HIV-1 gag polyprotein, according to the manufacturer's instructions. In order to release the gag protein from the enveloped VLPs, samples were incubated with SNCR buffer [44] at 70 °C for 10 min, followed by an incubation with 1.5% Triton X-100 at 100 °C for another 10 min. A linear calibration curve for the p24 protein (10 to 1000 pg/mL) was obtained using the HIV-1 p24 standard provided in the kit. A SIGMAFAST™ OPD substrate tablet (Sigma Aldrich, St. Louis, MO, USA) dissolved in 20 mL deionized water was used as substrate solution. The enzymatic reaction was stopped adding 1.25 N H_2SO_4. Absorbance was measured at 492 nm with a reference wavelength at 630 nm using an Infinite 200 Pro plate reader (Tecan, Männedorf, Switzerland).

2.11. Sodium dodecyl sulfate-polyacrylamide gel electrophoresis (SDS-PAGE) and Western blot analysis

Electrophoresis (200 V, 400 mA, 50 min) was performed in an X-cell SureLock® Mini-Cell electrophoresis chamber (Invitrogen, Carlsbad, CA, USA), using NuPAGE® Bis/Tris 4–12% gels (Invitrogen, Carlsbad, CA, USA) and reduced MES-SDS running conditions. Samples were prepared with NuPAGE® LDS sample buffer (Invitrogen, Carlsbad, CA, USA) and reduced at 99 °C for 15 min in the presence of 182 mM dithiothreitol (DTT). For each sample, a volume of 20 μL was loaded in a gel lane. SeeBlue® Plus2 Pre-stained Protein Standard (Invitrogen, Carlsbad, CA, USA) was used as molecular weight marker. Protein bands in the gel were stained using Coomassie Brilliant Blue G-250 based EZBlue™ Gel Staining Reagent (Sigma Aldrich, St. Louis, MO, USA). For Western blot analysis, after SDS-PAGE, proteins were transferred from the gel to a 0.2 μm nitrocellulose membrane using the Trans-Blot® Turbo™ Transfer System (Bio-Rad Laboratories, Hercules, CA, USA) according to the manufacturer's instructions. Membrane was blocked overnight with 3% w/v BSA in PBS-T (0.1% w/v Tween-20 in PBS). HIV-1 p24 detection was performed using a two-step procedure. First, the membrane was incubated with primary mouse monoclonal antibody against HIV-1 p24 (Icosagen AS, Tartumaa, Estonia), diluted 1:1000 in PBS-T containing 1% w/v BSA for 2 h. The second step was the incubation of the membrane with anti-mouse IgG conjugated with alkaline phosphatase (Sigma Aldrich, St. Louis, MO, USA), diluted 1:1000 in PBS-T with 1% w/v BSA for 1 h. Premixed BCIP®/NBT solution (Sigma Aldrich, St. Louis, MO, USA) was used as substrate for visualizing the alkaline phosphatase conjugates.

2.12. Transmission electron microscopy (TEM)

For nanoparticle visualization using TEM, relevant samples were prepared using the negative staining method. Briefly, 30 μL of sample were incubated on 400-mesh copper grids (coated with pioloform film and stabilized by carbon evaporation) for 1 min at room temperature. After the incubation, excess liquid was removed and samples were fixed incubating the grids with 2.5% glutaraldehyde solution (in 100 mM cacodylate buffer, pH 7.0) for 15 min. The grids were then washed with water and stained with 1% uranyl acetate solution for 30 s. After the staining, excess liquid was removed and the grids were air-dried. A Tecnai G^2 200 kV transmission electron microscope (FEI, Eindhoven, The Netherlands) was used for visualization of the specimens.

For cryo-TEM, approximately 4 μL of the sample were applied to a glow-discharged holey carbon grid and plunged frozen in liquid ethane using a FEI Vitrobot mark IV. Imaging was performed on an FEI F20 microscope at 200 kV and recorded on an FEI Ceta detector.

For observation of the internal structure of virgin and saturated beads, resin samples were washed and equilibrated with binding buffer (50 mM HEPES, pH 7.2). Saturated resins were prepared by incubating the resin beads with BSA or HIV-1 gag VLP in binding buffer, during 24 h at room temperature. After the incubation, beads were washed with binding buffer and chemically fixed with 2% glutaraldehyde for 20 min at room temperature. For the preparation of the specimens for TEM, resin samples were dehydrated with increasing ethanol concentrations (0–100% anhydrous ethanol), embedded in LRWhite resin (London Resin Company, Ltd., London, UK) and ultramicrotomed into 80 nm sections. The sections were then stained with lead citrate followed by uranyl acetate and imaged with a JEOL 1230 instrument (JEOL, Tokyo, Japan).

3. Results and discussion

3.1. Adsorption isotherms

HIV-1 gag VLP equilibrium binding capacity on Fractogel®-TMAE was determined and adsorption isotherms were constructed (Fig. 1). The Langmuir isotherm model [18] was applied to fit the experimental data. The obtained values for the maximum binding capacity (q_{max}) and equilibrium constant (K) are summarized in Table 1. Under strong binding conditions (50 mM HEPES, pH 7.2), a maximum binding capacity ($q_{max,0}$) of 1.6×10^{13} part/mL resin

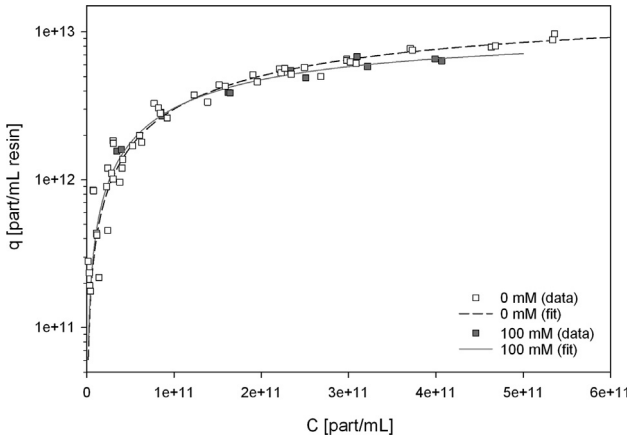

Fig. 1. Adsorption isotherms of HIV-1 gag VLPs on Fractogel®-TMAE after 24 h of incubation, using 0 or 100 mM NaCl in the binding buffer (50 mM HEPES, pH 7.2). Squares represent the data points and lines the fitting of the Langmuir isotherm model. C: equilibrium constant; q: surface concentration or binding capacity.

Table 1
Langmuir isotherm model parameters determined for the adsorption isotherms represented in Fig. 1. K: equilibrium constant; q_{max}: maximum binding capacity.

NaCl [mM]	K [mL/particles]	q_{max} [particles/mL resin]
0	2.4×10^{-12}	1.6×10^{13}
100	4.0×10^{-12}	1.1×10^{13}

was predicted. In order to evaluate the effect of moderate conductivity on binding, isotherms were also performed adding 100 mM NaCl to the binding buffer. This results in a conductivity similar to cell culture supernatants with 9.5–10.0 mS/cm. In this case, a maximum binding capacity ($q_{max,100}$) of 1.1×10^{13} part/mL resin was obtained. Despite $q_{max,100mM}$ value is 30% lower than $q_{max,0}$ it is important to note that particle concentrations measured by NTA have an accepted error of 20% [45,46]. Accordingly, no significant difference on binding capacity is observed under moderate conductivity conditions, allowing the direct loading of cell culture supernatant without compromising the binding capacity of the VLPs.

3.2. Breakthrough and dynamic binding capacity

The performance of Fractogel®-TMAE for the capture of HIV-1 gag VLPs was evaluated by the dynamic binding capacity ($DBC_{10\%}$) when directly loading 50 mL of 0.8 μm filtered cell culture

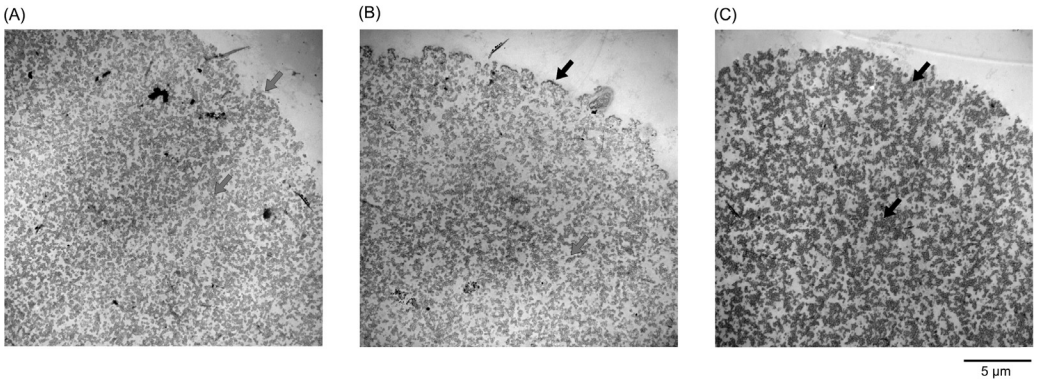

Fig. 2. Transmission electron micrographs of thin slices of (A) virgin, (B) VLP-saturated and (C) BSA-saturated Fractogel®-TMAE resin beads. Black arrow point to VLP/BSA bound to the resin and grey arrows point to free resin backbone.

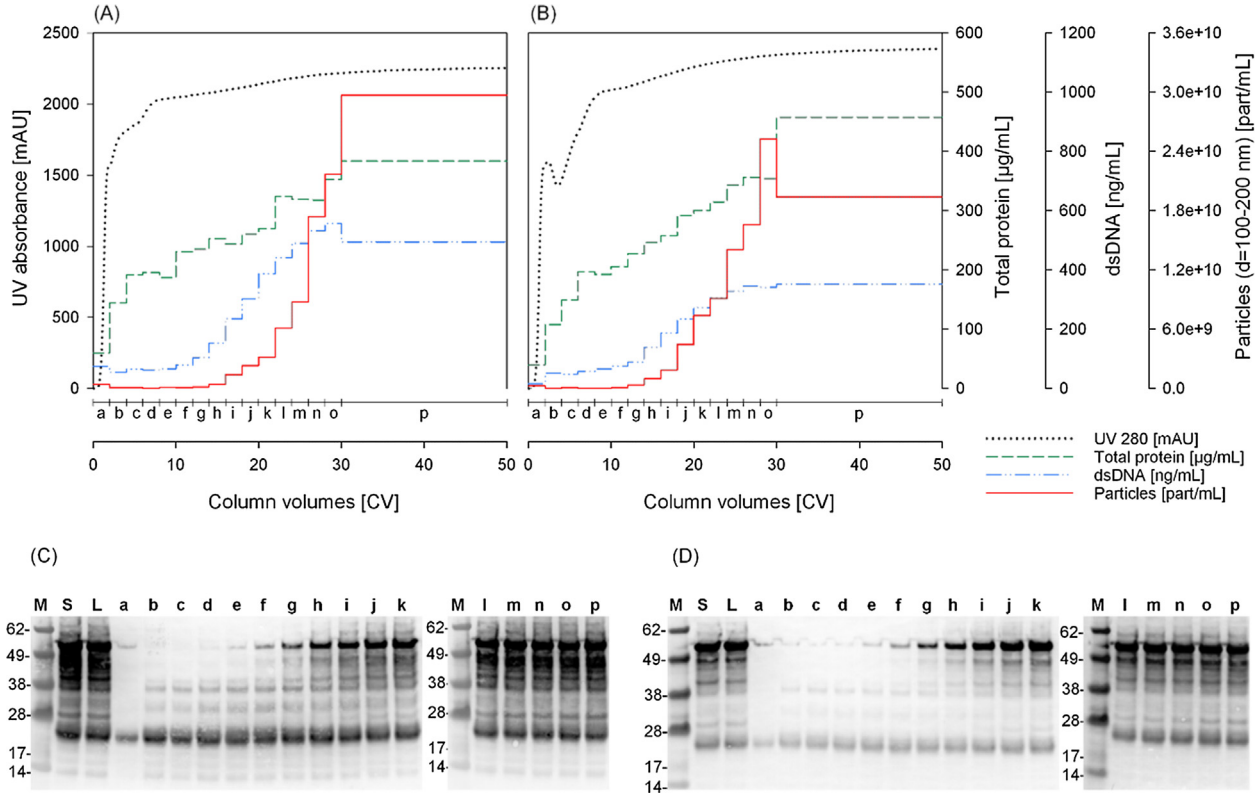

Fig. 3. (A) and (B) Breakthrough curves for the loading of CHO cell culture supernatant, containing HIV-1 gag VLPs, into 1 mL Fractogel®-TMAE MiniChrom columns. Total protein, dsDNA and particle concentrations were measured offline by Bradford, Picogreen and NTA, respectively; (C) and (D) Western blots for the detection of HIV-1 p24 corresponding to the breakthrough curves (A) and (B) respectively; (A) Loading material: 0.8 μm filtered CHO cell culture supernatant containing 710 μg/mL of total protein, 17594 ng/mL of dsDNA and 3.0×10^{10} part/mL of 100–200 nm particles; (B) Loading material: endonuclease treated and 0.8 μm filtered CHO cell culture supernatant containing 630 μg/mL of total protein, 441 ng/mL of dsDNA and 2.8×10^{10} part/mL of 100–200 nm particles; a-p: collected and analysed fractions.

supernatant onto a 1 mL column (Fig. 3A). In order to investigate the potential competition of dsDNA for the VLP binding sites, breakthrough experiments were also performed with endonuclease pretreated cell culture supernatant. The endonuclease digestion breaks down nucleic acids (DNA and RNA) into small oligonucleotides (3–5 bases) which can enter the resin pores, leaving the outer surface area of the beads available for VLP binding. dsDNA content was reduced by 97.9% (Fig. 3B). Collected flow-through fractions denoted as a-p (Fig. 3A and B) were analysed by NTA, Bradford assay and Picogreen assay for the quantification of particles, total protein and dsDNA respectively. In both cases, non-pretreated and endonuclease pretreated supernatant, proteins start to breakthrough immediately at 2 CV loading and 46–57% of the total protein did not bind to the column. This result was confirmed by the SDS-PAGE analysis (Fig. S1, Supplementary material A). This can be explained by the exclusion of positively-charged and non-charged proteins by the anion exchange ligands, as well as by the weak interaction with some negatively-charged proteins due to the moderate conductivity in the cell culture supernatant [3]. Nevertheless, full protein breakthrough was not achieved because the concentration at the outlet did not reach the feed concentration. In the non-pretreated supernatant (Fig. 3A), breakthrough of dsDNA and particles starts after about 12 and 14 CV loading respectively. Full breakthrough of particles is achieved at the end of the loading. However, only a 3% breakthrough of dsDNA is observed, indicating that the maximum binding capacity of Fractogel®-TMAE for dsDNA was not reached. Similar results were obtained for the endonuclease-pretreated supernatant (Fig. 3B). Western blot analysis (Fig. 3C and D) confirm the breakthrough of HIV-1 gag VLPs measured by NTA (bands at

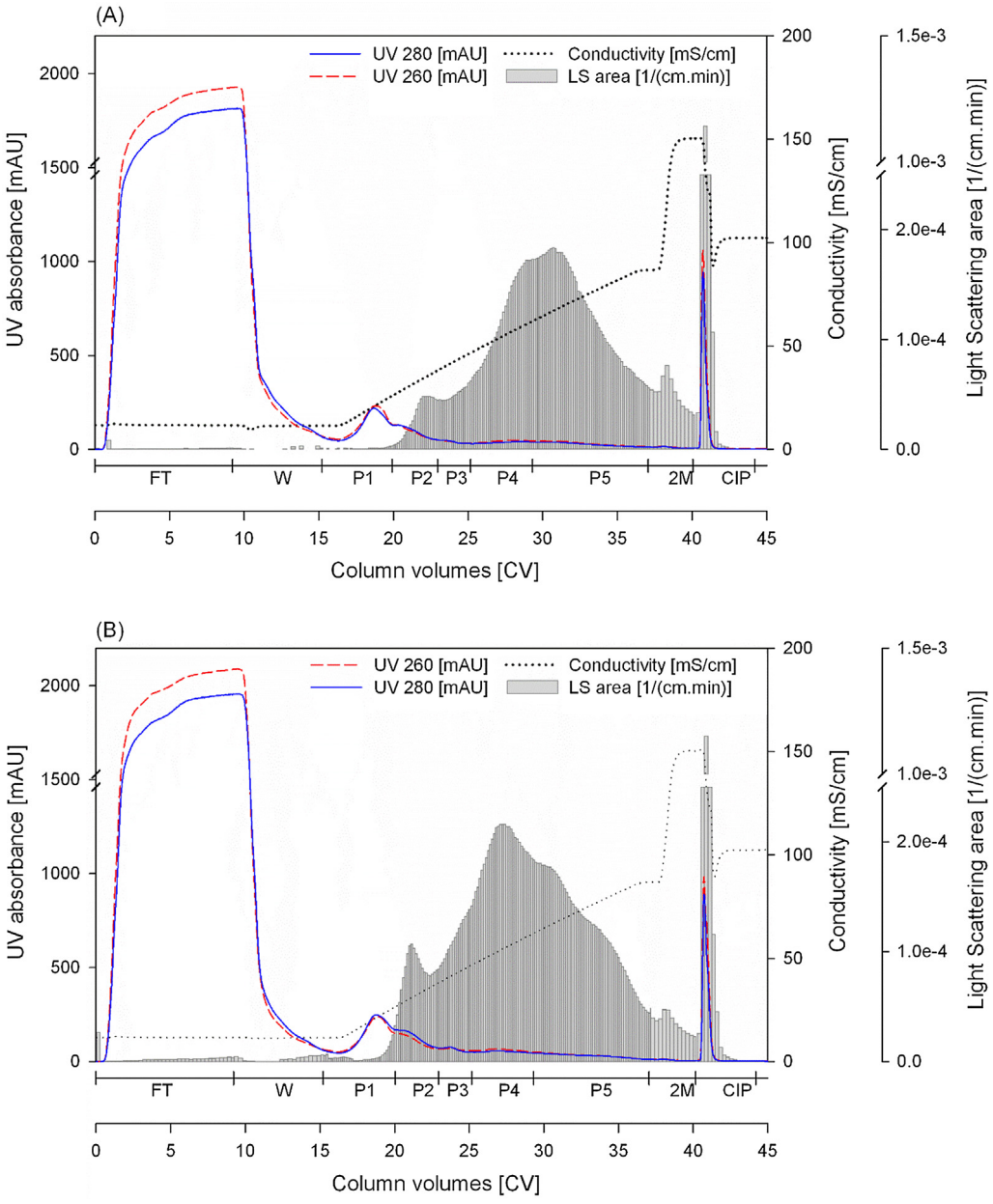

Fig. 4. Chromatograms of HIV-1 gag purification with Fractogel®-TMAE using a linear gradient elution from 100 to 1000 mM NaCl (Buffer A: 50 mM HEPES, pH 7.2; Buffer B: 50 mM HEPES, 2 M NaCl, pH 7.2). (A) Run 1: batch A. (B) Run 2: batch B. In both cases, the loading material was endonuclease pretreated and 0.8 μm filtered CHO cell culture supernatant. Bars represents the area under the curve of the light scattering intensity (LS) measurements for each collected fraction, using a MALS detector. FT: flow-through; W: wash; P1-5: peaks 1 to 5; 2 M: regeneration with 2 M NaCl; CIP: cleaning-in-place with 0.5 M NaOH.

55 kDa corresponding to HIV-1 gag polyprotein). $DBC_{10\%}$ was similar for both non-pretreated and endonuclease-pretreated supernatants with 6.6×10^{11} and 5.5×10^{11} part/mL column respectively, indicating that VLPs and dsDNA do not compete for the same binding sites.

Due to their large size, VLPs are expected to bind exclusively at the outer surface of the chromatography beads. Consequently, very low binding capacity would be expected. The exclusive binding of VLPs on the beads' outer surface was confirmed by transmission electron micrographs of VLP-saturated Fractogel®-TMAE beads (Fig. 2B). In Fig. 2, the uniform light grey area (outside and inside the beads) is the LRWhite embedding matrix, which fills the empty spaces. The medium-dark grey areas present in all images correspond to the resin backbone. When beads are incubated with a small protein (BSA), binding can be observed across the entire bead by the darker grey colour around the resin backbone (Fig. 2C). On the other hand, it is possible to observe that VLPs form a thin layer at the surface of the bead and no binding can be observed in the interior of the bead (Fig. 2B). This was also confirmed by confocal laser scanning microscopy when using fluorescently labelled VLPs (data not shown). Furthermore, it is possible to observe that despite being spherical, the beads have a rough surface, which increases the available surface area for VLP binding and is the explanation for obtaining a binding capacity higher than expected. The obtained dynamic binding capacity is only one order of magnitude smaller compared to the values reported for enveloped virus and VLPs on monoliths [38,47,48]. Additionally, since chromatography packed beds are scalable to hundreds of litres, the lower capacity of polymer-grafted media can be easily compensated by increasing the unit operation scale.

3.3. Purification of HIV-1 gag VLPs

Purification of HIV-1 gag VLPs produced in CHO cells was performed using a XK 16/20 column packed with 5.4 mL of Fractogel®-TMAE. Since the equilibrium binding capacity was not affected by moderate salt concentrations, clarified and 0.8 μm filtered cell culture supernatant was directly loaded onto the column. A loading volume of 50 mL was used to avoid column overloading and product loss. Elution was achieved using a 20 CV salt linear gradient from 100 to 1000 mM NaCl. The flow rate was 1 mL/min, ensuring a residence time of 5.4 min. Small fractions (0.8–1.5 mL) were collected throughout the entire chromatographic run and directly injected into a MALS detector using an HPLC in bypass mode (Fig. 4 and Fig. S2 (Supplementary material A)). The UV absorbance peak at 260 and 280 nm at the fractions were the majority of the particles elute is significantly reduced when the supernatant is pretreated with endonuclease (Fig. S2B). This indicates that the amount of dsDNA co-eluting with particles was reduced. Although pre-treatment of the supernatant with endonuclease does not increase the dynamic binding capacity, it is still required to reduce dsDNA contamination of the product. Consequently, further process development was performed with endonuclease pretreated supernatant.

Chromatograms in Fig. 4A and B represent two purification runs of HIV-1 gag VLPs from two different CHO cell culture batches (run 1/batch A and run 2/batch B respectively). Supernatant (S) from batch B had slightly higher content in particles and dsDNA and double the amount of total protein (Table 2). Before loaded onto the column both supernatants were pretreated with endonuclease and 0.8 μm filtered. Reductions of 98.2% and 97.1% in dsDNA content were achieved for batch A and B respectively. As before, small fractions were collected throughout the entire chromatographic runs and, directly after the run, analysed using a MALS detector. Fractions were later pooled, considering both UV absorbance and light scattering signals (Fig. 4A and B). To evaluate the purification process in terms of recovery, yield and host cell protein and dsDNA depletion, all collected fractions as well as loading materials were analysed for particle quantity, particle size distribution, total protein content, dsDNA content and HIV-1 gag protein content (Table 2). Additionally, the purity of the samples at the protein level was semi-quantitatively determined by SDS-PAGE (Fig. 5A

Table 2
Mass balance of HIV-1 gag purification with Fractogel®-TMAE represented in Fig. 4 (batch A: Fig. 4A; batch B: Fig. 4B). Particle, total protein, dsDNA and p24 concentrations measured by NTA, Bradford, Picogreen and p24 ELISA respectively. Recovery was calculated based on the particle concentration measured by NTA. S: supernatant; L: load; FT: flow-through; W: wash; P1-5: peaks 1 to 5; 2 M: regeneration with 2 M NaCl; CIP: cleaning-in-place with 0.5 M NaOH; < LLOQ: lower than the lower limit of quantification.

	Volume [mL]	Particles d: 100–200 nm [particles/mL]	Recovery [%]	Total Protein [μg/mL]	dsDNA [ng/mL]	p24 [ng/mL]
Batch A						
S	50.0	4.6×10^{10}	–	383.5	12096.9	2589.9
L	50.0	3.0×10^{10}	100.0	323.5	218.4	2473.9
FT	50.0	5.3×10^{08}	1.8	123.6	35.5	4.5
W	32.6	4.4×10^{08}	1.0	59.2	12.3	134.3
P1	25.5	<LLOQ	–	108.9	10.8	<LLOQ
P2	16.5	3.1×10^{09}	3.5	151.6	25.2	21.5
P3	12.0	2.6×10^{09}	2.1	40.6	31.6	140.2
P4	22.5	6.8×10^{09}	10.3	<LLOQ	384.2	324.8
P5	42.1	7.3×10^{09}	20.7	<LLOQ	61.1	274.1
2M	16.3	2.6×10^{09}	2.8	<LLOQ	13.3	102.8
CIP	26.0	1.9×10^{10}	32.6	81.8	<LLOQ	0.5
Total			74.7			
Batch B						
S	50.0	5.1×10^{10}	–	669.0	13720.5	2624.6
L	50.0	4.9×10^{10}	100.0	649.5	400.3	2342.0
FT	50.0	<LLOQ	–	172.7	47.9	893.7
W	32.6	<LLOQ	–	71.4	17.3	179.7
P1	26.3	<LLOQ	–	163.5	14.0	0.6
P2	15.8	3.7×10^{09}	2.4	312.1	60.8	130.0
P3	12.0	7.0×10^{09}	3.4	88.8	608.9	244.7
P4	22.5	1.2×10^{10}	11.4	<LLOQ	762.2	496.6
P5	42.1	1.0×10^{10}	17.8	<LLOQ	82.5	218.5
2M	16.3	3.1×10^{09}	2.1	<LLOQ	17.4	58.0
CIP	26.0	1.7×10^{10}	18.6	93.0	18.6	0.6
Total			55.8			

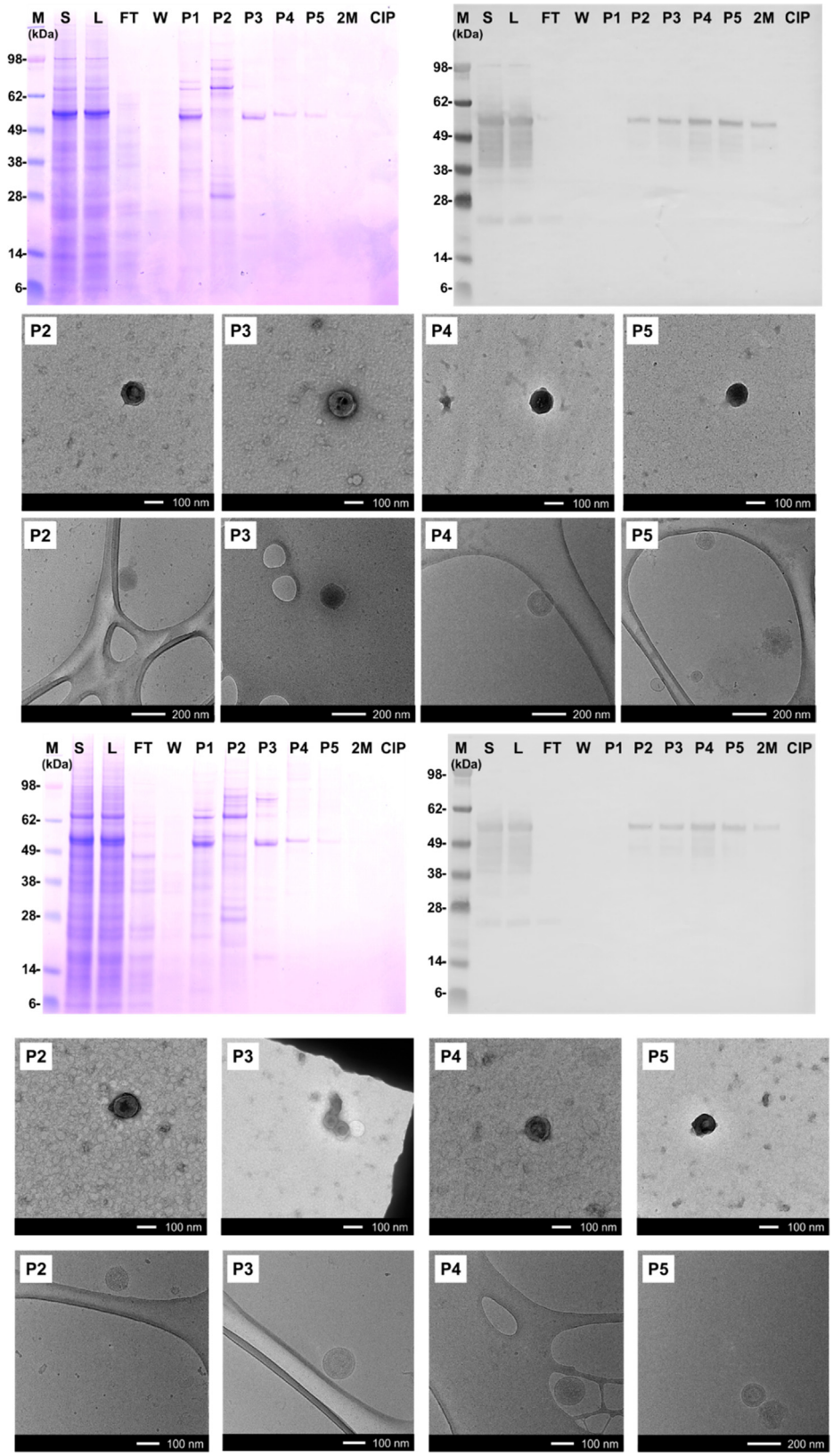

Fig. 5. (A) SDS-PAGE, (B) Western blot analysis, (C) TEM pictures and (D) cryo-TEM pictures of the pooled fractions from the purification run represented in Fig. 4A. (E) SDS-PAGE, (F) Western blot analysis, (G) TEM pictures and (H) cryo-TEM pictures of the pooled fractions from the purification run represented in Fig. 4B. M: molecular weight marker; S: supernatant; L: load; FT: flow-through; W: wash; P1-5: peaks 1 to 5; 2 M: regeneration with 2 M NaCl; CIP: cleaning-in-place with 0.5 M NaOH.

and E). MALS showed that almost all particles bound to the column. No significant light scattering signal is observed during column loading and washing, indicating no particle breakthrough (Fig. 4A and B). This was confirmed by NTA measurements of the flow-through and wash samples (Table 2). Majority of the host cell proteins did not bind to the column and were found in the flow-through and wash fractions. Bound proteins started to elute immediately at the beginning of the salt linear gradient and no particles were found in the first peak (P1). Particles were eluted in peaks 2 to 5 over a broad range of salt concentrations, starting from 320 mM NaCl (26 mS/cm) until the end of the linear gradient (1000 mM, 88 mS/cm). VLPs are large biomolecules and expose multiple host cell glycoproteins on their membrane. This complex surface allows the interaction with multiple ligands, resulting in a strong adsorption which requires high salt concertation for elution. This is different to protein elution, which requires lower salt concentrations, and lot of protein already eluted at binding conditions for VLPs. The non- or weakly-binding of protein impurities at moderate-high conductivities is one of the advantages of the use of polymer-grafted media to capture enveloped VLPs, which still bind to the column under these conditions.

HIV-1 gag polyprotein (55 kDa) was detected by Western blot analysis (Fig. 5B and F) in all particle-containing fractions, indicating the presence of HIV-1 gag VLPs. The presence of spherical particles in these fractions was confirmed by TEM (Fig. 5C and G). Cryo-TEM was used to investigate the inner structure of the particles (Fig. 5D and H). The majority of the particles had an outer membrane and appeared to be full. In some cases (Figs. 5D-P4 and 5H-P3) a second inner layer typical of HIV-1 gag VLPs was visible [49]. However, due to the concentration limitation of the scale, a low number of particles was found in the cryo-EM experiments therefore we can only speculate that structurally different particles are eluted in different fractions. Most particles in all peaks have a diameter of about 150 nm expressed as the statistical mode of the particle size distribution. The diameter of 150 nm is typical for HIV-1 gag VLPs [50]. However, peak 2 has a wider size distribution which is typical of EV samples [51]. Considering particle size distribution, SDS-page profile and p24 content, we assume that HIV-1 gag VLPs are enriched in the later fractions of the elution gradient in peaks 4 and 5. These two peaks contain the majority of the eluted particles and present a high purity at the protein level (Table 2, Fig. 5A and E). Yet, the depletion of dsDNA did not meet the requirements of the regulatory agencies (<10 ng/dose, dose: 10^9 particles).

3.4. Particle variants by proteomic analysis

Proteomic analysis of the different elution peaks was performed using LC-ESI-MS. The generated data were analysed by UnitProt database (detailed results are presented in Supplementary material B). Considering peaks 2 to 5, in total 214 and 227 proteins were identified in runs 1 and 2 respectively. Peak 2 had the highest number of total and unique proteins when compared with peaks 3 to 5. This is in agreement with the SDS-PAGE (Fig. 5A and E) as well as with the total protein concentration measured by Bradford. Nonetheless, Peak 2 is excluded from the proteomic interpretation, because it is contaminated by host cell proteins as seen in TEM and cryo-TEM. Peaks 3 to 5 have a substantial number of unique proteins (Table 3). Therefore, we assume that VLP variants are eluted. This is also supported by the particle size distribution measured for the different elution fractions. Previously it has been shown that HIV-1 uses different biogenesis pathways for budding [32]. This explains the presence of different particle variants. Moreover, peaks 2 and 3 have a wider particle size distribution than 4 and 5. Finally, we assume that numerous particle variants with similar surface properties and cargo are present and it is almost impossible to isolate single variants.

Table 3
Number of proteins identified by proteomic analysis using LC-ESI-MS.

Batch	Total P2-P5	Total P3-P5	Peak	Total	Unique	In P3-P5
A	214	111	**2**	145	103	21
			3	78	33	
			4	49	7	
			5	50	11	
B	227	129	**2**	163	98	30
			3	71	14	
			4	74	10	
			5	78	15	

High-resolution separation between different particle variants is crucial to allow the development of new analytical tools for high throughput particle quantification, characterisation and discrimination.

4. Conclusion

Our work demonstrates that polymer-grafted ion exchangers are suitable for the direct capture and purification of eVLPs. The developed method also allowed the separation of different HIV-1 gag VLP variants. Despite the binding capacity is one order of magnitude lower than the one for monoliths, chromatography columns can be packed in any size and geometry, allowing an easy and flexible scale-up. The strong VLP interaction versus the weak interaction of protein impurities is an advantage of this method because loading can be done at moderated salt concentrations, allowing direct loading of cell culture supernatants. The fact that VLPs bind exclusively on the outer surface leaves space on the interior of the beads available for the binding of highly negatively charged small impurities. Non-charged and positively charged proteins are immediately excluded from the column in the flow-through and wash steps, significantly improving product purity in a single step. This method can be easily implemented either in existing processes or adapted for the capture and purification of other enveloped VLPs produced in any type of expression system.

Declaration of Competing Interest

The authors declared that there is no conflict of interest.

Acknowledgements

This project has been supported by the Austrian Science Fund (project BioToP; FWF W1224). Schneider and Wetter have been supported by the Austrian BMWD, BMVIT, SFG, Standortagentur Tirol, Government of Lower Austria and Business Agency Vienna through the Austrian FFG-COMET-Funding Program. This work used the platforms of the Grenoble Instruct-ERIC Center (ISBG: UMS 3518 CNRS-CEA-UGA-EMBL) with support from FRISBI (ANR-10-INSB-05-02) and GRAL (ANR-10-LABX-49-01) within the Grenoble Partnership for Structural Biology (PSB). The electron microscope facility is supported by the Auvergne Rhône-Alpes Region, the Fondation Recherche Medicale (FRM), the fonds FEDER and the GIS-Infrastrutures en Biologie Sante et Agronomie, France (IBISA). The funding agencies had no influence on the conduct of this research. The authors would like to specially thank Professor Giorgio Carta for the great scientific collaboration and Preston Fuks for the help in the laboratory, especially regarding the imaging of resin beads.

Appendix A. Supplementary material

Supplementary data to this article can be found online at https://doi.org/10.1016/j.vaccine.2019.07.001.

References

[1] Lenhoff AM. Protein adsorption and transport in polymer-functionalized ion-exchangers. J Chromatogr A 2011;1218(49):8748–59. https://doi.org/10.1016/j.chroma.2011.06.061.

[2] Abdulrahman A, Ghanem A. Recent advances in chromatographic purification of plasmid DNA for gene therapy and DNA vaccines: A review. Anal Chim Acta 2018;1025:41–57. https://doi.org/10.1016/j.aca.2018.04.001.

[3] Zhu M, Fuks P, Carta G. Protein adsorption in anion exchange resins – effects of polymer grafting, support structure porosity, and protein size. Chem Technol Biotechnol 2018;93(7):1948–58. https://doi.org/10.1002/jctb.5410.

[4] Jungbauer A. Chromatographic media for bioseparation. J Chromatogr A 2005;1065(1):3–12. https://doi.org/10.1016/j.chroma.2004.08.162.

[5] Brune KD, Howarth M. New routes and opportunities for modular construction of particulate vaccines: stick, click, and glue. Front Immunol 2018;9(1432). https://doi.org/10.3389/fimmu.2018.01432.

[6] Ding X, Liu D, Booth G, Gao W, Lu Y. Virus-like particle engineering: from rational design to versatile applications. Biotech J 2018;13(5):1700324. https://doi.org/10.1002/biot.201700324.

[7] Donaldson B, Lateef Z, Walker GF, Young SL, Ward VK. Virus-like particle vaccines: immunology and formulation for clinical translation. Expert Rev Vaccines 2018;17(9):833–49. https://doi.org/10.1080/14760584.2018.1516552.

[8] Effio CL, Hubbuch J. Next generation vaccines and vectors: Designing downstream processes for recombinant protein-based virus-like particles. Biotech J 2015;10(5):715–27. https://doi.org/10.1002/biot.201400392.

[9] Pitoiset F, Vazquez T, Bellier B. Enveloped virus-like particle platforms: vaccines of the future? Expert Rev Vaccines 2015;14(7):913–5. https://doi.org/10.1586/14760584.2015.1046440.

[10] Watson DS, Endsley AN, Huang L. Design considerations for liposomal vaccines: Influence of formulation parameters on antibody and cell-mediated immune responses to liposome associated antigens. Vaccine 2012;30(13):2256–72. https://doi.org/10.1016/j.vaccine.2012.01.070.

[11] Hardcastle N, Boulis NM, Federici T. AAV gene delivery to the spinal cord: serotypes, methods, candidate diseases, and clinical trials. Expert Opin Biol Ther 2018;18(3):293–307. https://doi.org/10.1080/14712598.2018.1416089.

[12] Wolf MW, Reichl U. Downstream processing of cell culture-derived virus particles. Expert Rev Vaccines 2011;10(10):1451–75. https://doi.org/10.1586/erv.11.111.

[13] Turnbull J, Wright B, Green NK, Tarrant R, Roberts I, Hardick O, et al. Adenovirus 5 recovery using nanofiber ion-exchange adsorbents. Biotechnol Bioeng 2019;116(7):1698–709. https://doi.org/10.1002/bit.26972.

[14] Zöchling A, Hahn R, Ahrer K, Urthaler J, Jungbauer A. Mass transfer characteristics of plasmids in monoliths. J Sep Sci 2004;27(10–11):819–27. https://doi.org/10.1002/jssc.200401777.

[15] Marcus RK. Use of polymer fiber stationary phases for liquid chromatography separations: Part II – applications. J Sep Sci 2009;32(5–6):695–705. https://doi.org/10.1002/jssc.200800645.

[16] Ghosh R. Protein separation using membrane chromatography: opportunities and challenges. J Chromatogr A 2002;952(1):13–27. https://doi.org/10.1016/S0021-9673(02)00057-2.

[17] Nestola P, Peixoto C, Silva RRJS, Alves PM, Mota JPB, Carrondo MJT. Improved virus purification processes for vaccines and gene therapy. Biotechnol Bioeng 2015;112(5):843–57. https://doi.org/10.1002/bit.25545.

[18] Carta GA. Jungbauer Protein Chromatography: Process Development and Scale-Up. Weinheim: Wiley-VHC Verlag GmbH & Co. KGaA; 2010.

[19] Müller E. Properties and Characterization of High Capacity Resins for Biochromatography. Chem Eng Tech 2005;28(11):1295–305. https://doi.org/10.1002/ceat.200500161.

[20] Braas G, Searle PF, Slater NKH, Lyddiatt A. Strategies for the isolation and purification of retroviral vectors for gene therapy. Bioseparation 1996;6(4):211–28.

[21] Yu M, Li Y, Zhang S, Li X, Yang Y, Chen Y, et al. Improving stability of virus-like particles by ion-exchange chromatographic supports with large pore size: Advantages of gigaporous media beyond enhanced binding capacity. J Chromatogr A 2014;1331:69–79. https://doi.org/10.1016/j.chroma.2014.01.027.

[22] Yamamoto S, Miyagawa E. Retention behavior of very large biomolecules in ion-exchange chromatography. J Chromatogr A 1999;852(1):25–30. https://doi.org/10.1016/S0021-9673(99)00594-4.

[23] Wu Y, Simons J, Hooson S, Abraham D, Carta G. Protein and virus-like particle adsorption on perfusion chromatography media. J Chromatogr A 2013;1297:96–105. https://doi.org/10.1016/j.chroma.2013.04.062.

[24] Trilisky EI, Lenhoff AM. Sorption processes in ion-exchange chromatography of viruses. J Chromatogr A 2007;1142(1):2–12. https://doi.org/10.1016/j.chroma.2006.12.094.

[25] Bowes BD, Koku H, Czymmek KJ, Lenhoff AM. Protein adsorption and transport in dextran-modified ion-exchange media. I: Adsorption. J Chromatogr A 2009;1216(45):7774–84. https://doi.org/10.1016/j.chroma.2009.09.014.

[26] Almodóvar EXP, Tao Y, Carta G. Protein adsorption and transport in cation exchangers with a rigid backbone matrix with and without polymeric surface extenders. Biotechnol Prog 2011;27(5):1264–72. https://doi.org/10.1002/btpr.643.

[27] Bowes BD, Lenhoff AM. Protein adsorption and transport in dextran-modified ion-exchange media. III. Effects of resin charge density and dextran content on adsorption and intraparticle uptake. J Chromatogr A 2011;1218(40):7180–8. https://doi.org/10.1016/j.chroma.2011.08.039.

[28] Wang Q, Yu L, Sun Y. Grafting glycidyl methacrylate to Sepharose gel for fabricating high-capacity protein anion exchangers. J Chromatogr A 2016;1443:118–25. https://doi.org/10.1016/j.chroma.2016.03.033.

[29] Müller W. New ion exchangers for the chromatography of biopolymers. J Chromatogr A 1990;510:133–40. https://doi.org/10.1016/S0021-9673(01)93746-X.

[30] Diedrich J, Heymann W, Leweke S, Hunt S, Todd R, Kunert C, et al. Multi-state steric mass action model and case study on complex high loading behavior of mAb on ion exchange tentacle resin. J Chromatogr A 2017;1525:60–70. https://doi.org/10.1016/j.chroma.2017.09.039.

[31] Shirbaghaee Z, Bolhassani A. Different applications of virus-like particles in biology and medicine: Vaccination and delivery systems. Biopolymers 2015;105(3):113–32. https://doi.org/10.1002/bip.22759.

[32] Welsch S, Müller B, Kräusslich H-G. More than one door – Budding of enveloped viruses through cellular membranes. FEBS Lett 2007;581(11):2089–97. https://doi.org/10.1016/j.febslet.2007.03.060.

[33] Kurg R, Reinsalu O, Jagur S, Õunap K, Võsa L, Kasvandik S, et al. Biochemical and proteomic characterization of retrovirus Gag based microparticles carrying melanoma antigens. Sci Rep 2016;6:29425. https://doi.org/10.1038/srep29425.

[34] McCraw DM, Gallagher JR, Torian U, Myers ML, Conlon MT, Gulati NM, et al. Structural analysis of influenza vaccine virus-like particles reveals a multicomponent organization. Sci Rep 2018;8(1):10342. https://doi.org/10.1038/s41598-018-28700-7.

[35] Onafuwa-Nuga AA, Telesnitsky A, King SR. 7SL RNA, but not the 54-kd signal recognition particle protein, is an abundant component of both infectious HIV-1 and minimal virus-like particles. RNA 2006;12(4):542–6. https://doi.org/10.1261/rna.2306306.

[36] Nolte-'t Hoen E, Cremer T, Gallo RC, Margolis LB. Extracellular vesicles and viruses: Are they close relatives? Proc Natl Acad Sci USA 2016;113(33):9155–61. https://doi.org/10.1073/pnas.1605146113.

[37] Michen B, Graule T. Isoelectric points of viruses. J Appl Microbiol 2010;109(2):388–97. https://doi.org/10.1111/j.1365-2672.2010.04663.x.

[38] Steppert P, Burgstaller D, Klausberger M, Berger E, Aguilar PP, Schneider TA, et al. Purification of HIV-1 gag virus-like particles and separation of other extracellular particles. J Chromatogr A 2016;1455:93–101. https://doi.org/10.1016/j.chroma.2016.05.053.

[39] Vicente T, Roldão A, Peixoto C, Carrondo MJT, Alves PM. Large-scale production and purification of VLP-based vaccines. J Invertebr Pathol 2011;107:S42–8. https://doi.org/10.1016/j.jip.2011.05.004.

[40] Thompson CM, Petiot E, Lennaertz A, Henry O, Kamen AA. Analytical technologies for influenza virus-like particle candidate vaccines: challenges and emerging approaches. Virol J 2013;10(1):141. https://doi.org/10.1186/1743-422x-10-141.

[41] Tengattini S. Chromatographic approaches for purification and analytical characterization of extracellular vesicles: recent advancements. Chromatographia 2018. https://doi.org/10.1007/s10337-018-3637-7.

[42] Tang VA, Renner TM, Fritzsche AK, Burger D, Langlois M-A. Single-particle discrimination of retroviruses from extracellular vesicles by nanoscale flow cytometry. Sci Rep 2017;7(1):17769. https://doi.org/10.1038/s41598-017-18227-8.

[43] Gutiérrez-Granados S, Cervera L, Gòdia F, Carrillo J, Segura MM. Development and validation of a quantitation assay for fluorescently tagged HIV-1 virus-like particles. J Virol Methods 2013;193(1):85–95. https://doi.org/10.1016/j.jviromet.2013.05.010.

[44] Schüpbach J, Tomasik Z, Knuchel M, Opravil M, Günthard HF, Nadal D, et al. Optimized virus disruption improves detection of HIV-1 p24 in particles and uncovers a p24 reactivity in patients with undetectable HIV-1 RNA under long-term HAART. J Med Virol 2006;78(8):1003–10. https://doi.org/10.1002/jmv.20655.

[45] U.S. Department of Health and Human Services Food and Drug Administration Guidance for Industry, Bioanalytical Method Validation. In: Center for Drug Evaluation and Research (CDER) Center for Veterinary Medicine (CVM); 2001.

[46] Kramberger P, Ciringer M, Štrancar A, Peterka M. Evaluation of nanoparticle tracking analysis for total virus particle determination. Virol J 2012;9(1):265. https://doi.org/10.1186/1743-422x-9-265.

[47] Gerster P, Kopecky E-M, Hammerschmidt N, Klausberger M, Krammer F, Grabherr R, et al. Purification of infective baculoviruses by monoliths. J Chromatogr A 2013;1290:36–45. https://doi.org/10.1016/j.chroma.2013.03.047.

[48] Steppert P, Burgstaller D, Klausberger M, Kramberger P, Tover A, Berger E, et al. Separation of HIV-1 gag virus-like particles from vesicular particles impurities

by hydroxyl-functionalized monoliths. J Sep Sci 2017;40(4):979–90. https://doi.org/10.1002/jssc.201600765.
[49] Wang B-Z, Liu W, Kang S-M, Alam M, Huang C, Ye L, et al. Incorporation of high levels of chimeric human immunodeficiency virus envelope glycoproteins into virus-like particles. J Virol 2007;81(20):10869–78. https://doi.org/10.1128/jvi.00542-07.
[50] Steppert P, Burgstaller D, Klausberger M, Tover A, Berger E, Jungbauer A. Quantification and characterization of virus-like particles by size-exclusion chromatography and nanoparticle tracking analysis. J Chromatogr A 2017;1487:89–99. https://doi.org/10.1016/j.chroma.2016.12.085.
[51] Raposo G, Stoorvogel W. Extracellular vesicles: exosomes, microvesicles, and friends. J Cell Biol 2013;200(4):373–83. https://doi.org/10.1083/jcb.201211138.